A Thermodynamic Phase Transition in Magnetic Reconnection

J. Jara-Almonte and H. Ji
Princeton Plasma Physics Laboratory, Princeton, New Jersey 08543, USA
(Dated: June 28, 2021)

By examining the entropy production in fully kinetic simulations of collisional plasmas, it is shown that the transition from collisional, Sweet-Parker reconnection to collisionless, Hall reconnection may be viewed as a thermodynamic phase transition. The phase transition occurs when the reconnection electric field satisfies $E = E_D\sqrt{m_e/m_i}$, where m_e/m_i is electron-to-ion mass ratio and E_D is the Dreicer electric field. This condition applies for all m_i/m_e, including $m_i/m_e = 1$ where the Hall regime vanishes and a direct phase transition from the collisional to the kinetic regime occurs. In the limit $m_e/m_i \to 0$, this condition is equivalent to there being a critical electron temperature, $T_e \approx m_i\Omega_i^2\delta^2$ where Ω_i is ion cyclotron frequency and δ is the current sheet half-thickness. The heat capacity of the current sheet changes discontinuously across the phase transition, and a critical power law is identified in an effective heat capacity. A model for the time-dependent evolution of an isolated current sheet in the collisional regime is derived.

Magnetic reconnection is a fundamental plasma process responsible for rapidly releasing stored magnetic energy and changing the magnetic topology. Reconnection occurs in nearly all magnetized plasma environments from highly collisional, to nearly collisionless kinetic systems. A wide variety of physical effects and instabilities influence the reconnection process, such as the Hall effect [1], electron kinetic effects [2, 3], and plasmoid instabilities [4–6], many of which were empirically organized into a reconnection phase diagram in analog with a thermodynamic phase diagram [7].

While the reconnection phase diagram is a successful tool for organizing parameter space, the question of whether there truly exist phase transitions between different regimes has not been rigorously addressed. In reconnection, the simplest and most well-established regimes are the slow, collisional [8–11] and fast, collisionless regimes [1, 12, 13] with a single two-dimensional (2D) X-line. This Letter focuses solely on the fundamental physics of the transition between these two regimes.

Previous results for anti-parallel reconnection have suggested that the transition occurs when $\delta = d_i$ where δ is the current sheet half-thickness, $d_i \equiv c/\omega_{pi}$ is the ion inertial length, and ω_{pi} is the ion plasma frequency [14, 15]. The importance of d_i was suggested based on a scaling analysis of the generalized Ohm's law [16], the presence of fast, dispersive waves [17], and abundant empirical evidence that d_i is a relevant length scale within the collisionless regime [18]. However, there is no fully self-consistent, first-principles theory that describes the transition or justifies the exact equality $\delta = d_i$.

To-date, the most comprehensive model of the transition is the catastrophe model of Cassak *et al.* [14] who examined it in an isothermal two-fluid system. An evolution equation for the current sheet was developed and a bifurcation from the collisional to the Hall regimes was identified [19]. This model has hysteresis and it was argued that phase diagrams must therefore include history effects [20]. Hysteresis was observed in a two-fluid simulation by artificially modifying the resistivity [14], as well as in a Hall-MHD simulation due to the self-consistent interplay between plasmoid instability and Hall physics [21]. To the authors' knowledge, similar effects have not been observed in fully kinetic simulations, suggesting that the underlying physics of the transition may differ from simplified fluid models. Within kinetic simulations, the transition has been observed in both 2D and 3D and for both electron-positron and electron-ion plasmas [22–25], and dynamic thinning of Sweet-Parker current sheets due the Ohmic heating is known to be an important effect [24].

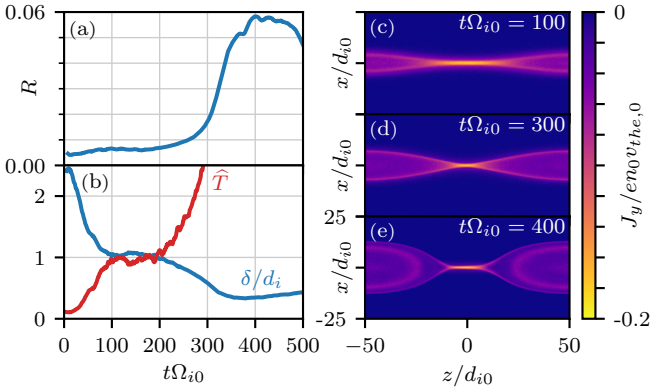

FIG. 1. (a) Reconnection rate and (b) δ/d_i and $\widehat{T}$ as a function of time. (c-e) Example out-of-plane current density in the (c) collisional, (d) Hall, and (e) kinetic regimes.

Here, these earlier results are extended by examining fully kinetic particle-in-cell (PIC) simulations that self-consistently evolve from an initial collisional equilibrium, through a Hall regime where electrons and ions are decoupled, but classical resistivity is the dominant non-ideal effect, and finally into a collisionless, kinetic regime. The evolution of the entropy is examined, and a thermodynamic phase transition is shown to exist between the collisional and Hall regimes. For finite m_i/m_e, electron gyroviscosity cannot be neglected, and the phase transition occurs when the normalized reconnection elec-

tric field satisfies $\widehat{E} \equiv E\sqrt{m_i/m_e}/E_D = 1$, where $E_D = m_e v_{the}\nu_{ei}/e$ is the Dreicer electric field, v_{the} is electron thermal speed, and ν_{ei} is electron-ion collision frequency. This condition applies for all m_i/m_e, including $m_i/m_e = 1$ where the Hall regime vanishes and a direct phase transition from the collisional to the kinetic regime occurs. In the limit $m_e/m_i \to 0$, and assuming a Sweet-Parker equilibrium, this condition reduces to $\rho_s/\delta = \beta_e/2 \approx 1$ where $\rho_s = \Omega_i^{-1}\sqrt{T_e/m_i}$ is the ion sound radius, Ω_i is the ion cyclotron frequency, and $\beta_e = 8\pi n_e T_e/B^2$ is the ratio of electron pressure to magnetic field pressure. This condition may also be written as $\widehat{T} \equiv T_e/m_i\Omega_i^2\delta^2 \approx 1$.

To further understand the phase transition, both the current sheet heat capacity, C, and an effective heat capacity, $\widehat{C}$, are introduced. C is discontinuous across the phase transition corresponding to a change from isobaric to isochoric heating, while $\widehat{C}$ obeys a critical power law. These results allow the time-dependent heating model of Stanier *et al.* [24] to be extended into the "nonlinear" regime where the phase transition occurs. It is shown that in idealized and closed systems, Sweet-Parker current sheets will always collapse down to kinetic scales provided there is enough free magnetic energy, and the collapse timescale only weakly depends on the initial current sheet thickness.

The PIC code VPIC [26, 27], along with a Coulomb collision algorithm [22, 28], is used to simulate reconnection in a resistive current sheet. The initial setup is a 1D Harris equilibrium with $\mathbf{B} = B_0\tanh(x/\delta_0)\widehat{z}$, $n_e = n_i = n_b + n_0\mathrm{sech}^2(x/\delta_0)$ and $T_i = T_e = m_i v_{A0}^2/4$ where $n_b/n_0 = 0.3$, $\delta_0 = 2d_{i0}$, $d_{i0}^2 \equiv m_i c^2/4\pi n_0 e^2$, and $v_{A0}^2 = B_0^2/4\pi(m_i + m_e)n_0$. An initial, long-wavelength perturbation is applied to seed reconnection. For the case discussed in detail, $m_i/m_e = 40$, $\omega_{pe,0}/\Omega_{e0} = 2$, and $\nu_{ei,0}/\Omega_{e0} \approx 0.042$, corresponding to an initial Lundquist number $S_0 = 4\pi L_0 v_{A,up}/\eta_0 c^2 \approx 2200$, where η_0 is the initial Spitzer resistivity, $v_{A,up}^2 = (n_0/n_b)v_{A0}^2$, and $L_0 = L_z/2$. The domain spans $L_x \times L_z = 50 \times 100 d_{i0}$ and contains 790×1560 cells and 2.5×10^9 macroparticles. Periodic boundary conditions are used along z, while particle reflecting and electrically conducting boundaries are used along x. The time dependence of the reconnection rate, $R = cE_y/Bv_A$, and δ/d_i are shown in Fig. 1, along with the out-of-plane current density at three representative times corresponding to the collisional, Hall, and kinetic regimes.

Thermodynamic phase transitions often involve change in the entropy or in properties derived from entropy and several previous studies have examined entropy in PIC simulations [29–32]. The differential (Boltzmann-Gibbs) entropy for a species s is given by

$$H_s(t) \equiv \int d^3x\, h_s(\mathbf{x},t), \quad h_s(\mathbf{x},t) \equiv -\int d^3v\, f_s \ln f_s \tag{1}$$

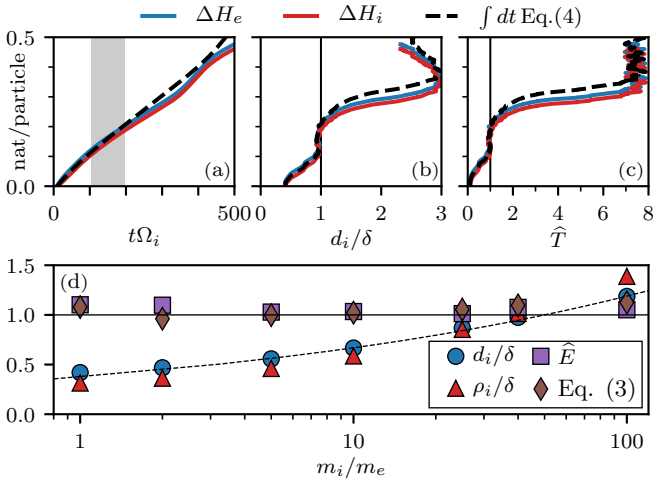

FIG. 2. (a-c) Evolution of the electron and ion differential entropy, H_e and H_i, relative to their initial value (a) as a function of time, and reorganized by (b) δ/d_i and (c) $\widehat{T}$. The identified phase transition is shaded in (a) and shown with a vertical line in (b-c). (d) Quantitative evaluation of proposed transition criteria at the time of the collisional to Hall (kinetic for $m_i/m_e = 1$) phase transition. The dotted line in shows a reference $(m_i/m_e)^{1/4}$ scaling.

where f_s is the single-particle distribution function for species s. Previous studies have used a plug-in integral estimator where h_s is integrated over a phase-space histogram [30, 32]. For the similar plug-in redistribution estimator, histograms are either slowly converging or inconsistent with significant bias [33], leading to non-negligible systematic error. Here, h_s is instead computed with the Kozachenko-Leonenko (KL) estimator [34],

$$h_s(\mathbf{x},t) = -wn\,[b(k) - b(n)] + w\sum_{i=1}^{n}\ln\left(\frac{4\pi\rho_{i,k}^3}{3kw}\right), \tag{2}$$

where $\rho_{i,k}$ is the distance in velocity space from macroparticle i to its k-th nearest neighbor and $b(x) = \psi(x) - \ln x$ where $\psi(x)$ is the digamma function. The sum extends over all n macroparticles in a given cell, each of which has an identical statistical weight w. The standard choice $k = 1$ is used here. KL is consistent and converges as $n^{-1/2}$ if f satisfies regularity conditions [35]. KL is compared with a histogram estimator in the Supplementary Information [36].

The time evolution of H_s is shown in Fig. 2(a). Entropy monotonically increases in time and at a rate larger than the numerical entropy gain in an equivalent collisionless case. To lowest order, entropy is equally partitioned between species since deviations from quasineutrality ($n_e = n_i$) and local thermal equilibrium ($T_e = T_i$) are small. To gain insight into the various regimes of reconnection, the data can be reorganized using the current sheet width rather than time as an independent coordinate, Fig. 2 (b-c). Two measures are shown, d_i/δ, where

δ is the half-width at half-max of J_y and d_i is evaluated using the X-point density, and $\widehat{T} \equiv T_e/m_i\Omega_i^2\delta^2$ where T_e is evaluated at the X-point and B at 1δ upstream. The former is motivated by significant heuristic and empirical evidence that d_i is involved in the transition physics, while the latter is a dimensionless temperature measure. In these simulations, $\widehat{T}$ predominantly changes due to current sheet thinning and may be equivalently viewed as a measure of δ.

An abrupt increase in H_s can be seen at $\delta \approx d_i \approx \rho_s$. This discontinuity in entropy could be interpreted as a first-order thermodynamic phase transition where the net change in entropy across the phase transition is due to a latent heat. However, the phase transition requires finite time, $100\Omega_{i0}^{-1} \lesssim t \lesssim 200\Omega_{i0}^{-1}$, in order to occur. During this time, ongoing reconnection leads to a continuous production of entropy unrelated to the phase transition itself. As will be shown below, the phase transition appears to be continuous.

By finding the local minimum in $|d(d_i/\delta)/dH_i|$, the point at which the collisional to Hall (kinetic for $m_i/m_e = 1$) phase transition occurs can be accurately determined. Various proposed transition criteria are shown as a function of m_i/m_e and at the time of the phase transition in Fig. 2(d). The criteria $\delta = d_i$ and $\delta = \rho_i$ do not hold for all mass ratios. Rather, it is empirically found that the local criteria $\widehat{E} \equiv E\sqrt{m_i/m_e}/E_D = 1$ is an accurate prediction of when the phase transition will occur across all m_i/m_e. This criteria was previously suggested as an equivalent condition to $\delta = \rho_s$ since for large m_i/m_e it can be written as $\rho_s/\delta_{SP} = \beta_e/2$ or $\widehat{T} = (\beta_e/2)^2$ where $\delta_{SP} = L/\sqrt{S}$ and L and S are the time-dependent half-length and Lundquist number of the current sheet [37].

For finite m_i/m_e however, $\widehat{E}$ differs from the large m_i/m_e limit due to electron gyroviscosity which is present even in the collisional regime. Within the current sheet, the electron pressure tensor, $\mathbf{P_e}$, has finite off-diagonal elements $P_{e,xy}$ and $P_{e,yz}$ due to electron motion in the sheared magnetic field [38]. In the steady-state, collisionless limit, $\partial P_{e,xy}/\partial x \approx \partial P_{e,yz}/\partial z$ resulting in an electric field $E_{NG} \equiv \sqrt{2}(m_e/e)v_{the}dv_{ez}/dz$ [39]. However, these simulations are in a semi-collisional regime where $L \gtrsim v_{the}/\nu_{ei} \gg \delta$. As a result, collisions suppress $P_{e,yz}$, but do not affect $P_{e,xy}$, and the electric field is reduced by half from the collisionless limit, $(\nabla \cdot \mathbf{P_e})_y/en \approx E_{NG}/2$. This effect is discussed further in the Supplementary Information [36]. Setting $dv_{ez}/dz = v_A/L$ gives $E_{NG}/2E_D = d_e^2/\sqrt{2}\delta_{SP}^2$ and the condition

$$\sqrt{\frac{m_i}{m_e}}\frac{\eta J_y + \frac{1}{2}E_{NG}}{E_D} = \frac{2}{\beta_e}\left(\frac{\rho_s}{\delta} + \sqrt{\frac{m_e}{2m_i}}\frac{\rho_s^2}{\delta_{SP}^2}\right) = 1, \quad (3)$$

where $\delta \neq \delta_{SP}$ in general. For $m_i/m_e \to \infty$, the Sweet-Parker limit is recovered, while for $m_i/m_e \to 1$, then $\rho_s/\delta_{SP} \sim (m_i/m_e)^{1/4}$. Eq. (3) is evaluated and shown to hold within 12% in Fig. 2(d). Although this correction vanishes in the large m_i/m_e limit, it provides insight into the underlying physics; the local electric field is responsible for the phase transition, not the current sheet geometry. The remainder of this Letter assumes $m_i/m_e \gg 1$ and $n_b/n_0 \ll 1$ which allows the simpler condition $\widehat{T} \approx 1$ to be used; up to factors of $\beta_e \sim 1$, this is equivalent to the slow-to-fast transition criteria in Cassak *et al.* [14].

In the collisional regime, the rate of entropy production can be estimated as $dH/dt = (1/T)dQ/dt$ where Q is the total heat generated by collisions. Locally, the heat generation is predominantly resistive dissipation, ηJ^2, and so $dH/dt \approx (4L\delta L_y)(\eta J^2/T) \approx 2N_{SP}\beta^{-1}\nu_{ie}\left(d_i/\delta\right)^2$ where ν_{ie} is the ion-electron collision frequency, $N_{SP} \equiv 4L\delta L_y n$ is the number of particles in the current sheet, and L_y is the out-of-plane extent. Assuming that L and B are constant and using the Spitzer resistivity scaling, $\eta \sim T^{-3/2}$ gives the scaling $S \sim n^{-1/2}T^{3/2} \sim \beta^{3/2}n^{-2}$. For Sweet-Parker current sheets it then follows that $N_{SP} \sim n\delta^2 S^{1/2} \sim \beta^{3/4}\delta^2$. Using the subscript 0 to denote initial condition values and taking $\beta \approx 1$ leads to the estimate

$$\frac{dH}{dt} \approx 2N_{SP,0}\left(\frac{\delta_{SP,0}}{\delta_0}\right)^2\left(\frac{T_0}{T}\right)^{3/2}\tau_{A0}^{-1}, \quad (4)$$

where $\tau_A \equiv L/v_A$ is the Alfvén transit time.

Using the X-line temperature and assuming $H_e \approx H_i$, Eq. (4) is integrated to produce the black dashed line in Fig. 2 (a-c) which agrees well with the simulation during the collisional phase, $t \lesssim 100\Omega_{i0}^{-1}$. In the collisionless regimes, resistive production of entropy is reduced and viscous heating and thermal mixing are additional sources of entropy production; these effects will be detailed further in a future manuscript.

To characterize the phase transition, the viscous electric fields at the X-point, ϕ_e and ϕ_i, are proposed as phenomenological order parameters,

$$\phi_s = -\left\langle \frac{c(\nabla \cdot \mathbf{P}_s)_y}{q_s n_s B_0 V_{A,0}} \right\rangle \quad (5)$$

where $\langle\cdot\rangle$ denotes local spatiotemporal averaging in order to reduce statistical noise. These order parameters are shown as a function of $\widehat{T}$ in Fig. 3(a). They are equivalent until the onset of kinetic effects ($\widehat{T} \sim 6$), which follows from the momentum equations since $\nabla \cdot (\mathbf{P_e} + \mathbf{P_i}) = 0$ at a symmetric, steady-state X-point. There is an onset at $\widehat{T} = 1$, corresponding to a transition from a disordered phase ($\widehat{T} < 1$) to an ordered phase ($\widehat{T} > 1$).

The heat capacity of a system changes across a thermodynamic phase transition. Here, two heat capacities are introduced, $C \equiv TdH/dT$ and $\widehat{C} \equiv \widehat{T}dH/d\widehat{T}$, where T is the X-point temperature and $H = H_e + H_i$. C and $\widehat{C}$ are shown in Fig. 3(b-c). C has a discontinuous change at $\widehat{T} = 1$ consistent with a continuous phase transition. $\widehat{C}$ is asymmetric and diverges at $\widehat{T} = 1$. For $\widehat{T} < 1$, there

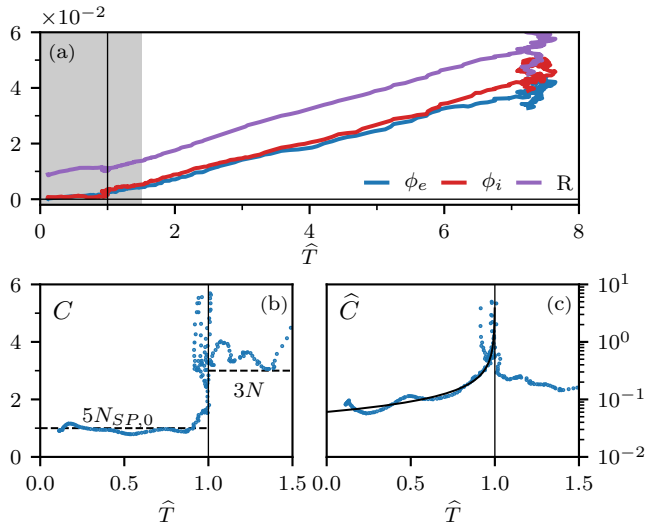

FIG. 3. Order parameters (a) and effective heat capacities (b-c) for the reconnection phase transition as a function of $\widehat{T}$. Vertical lines are drawn at $\widehat{T} = 1$ where a phase transition occurs. Shading in (a) shows the region examined in (b-c), dashed lines in (b) show different limits as discussed in the text, and the black line in (c) is a power law fit with critical exponent $\bar{\alpha} = -3/5$.

is a critical power law, $\widehat{C} \sim \alpha_0(1-\widehat{T})^{\bar{\alpha}}$, with the best fit scaling exponent $\bar{\alpha} = -3/5$.

The two limits for C can be understood. If there is efficient thermal transport across flux surfaces, then changing the X-point temperature requires heating the entire plasma volume. This is an isochoric process due to the fixed simulation volume, and $C \approx 3N$ where $N = \int d^3x\, n$ is the total number of (real) particles per species. A factor of 2 has been included to account for both species. This limit is consistent with the ordered-side. In the opposite limit, heat is confined within the current sheet and outflow. This is an isobaric process since the reconnecting magnetic field maintains a constant pressure within the current sheet and $C \approx 5(N_{SP} + N_{out})$ where N_{out} is the number of particles in the outflow. Since the initial equilibrium is a 1D current sheet, $N_{out,0} = 0$, and neglecting the contribution from inflowing particles gives $N_{SP,0} = N_{SP} + N_{out}$ and $C \approx C_0 \equiv 5N_{SP,0}$. This limit is consistent with the disordered-side of Fig. 3(b).

As an example of the utility of C and $\widehat{C}$, a model for the evolution of a resistive current sheet can be developed. Writing Eq. (4) as $dH/dt = H_0' T^{-3/2}$, and using the definition of C and $\widehat{C}$ gives

$$\frac{d\widehat{T}}{dt} = \frac{H_0'}{\alpha_0}\frac{\widehat{T}}{(1-\widehat{T})^{\bar{\alpha}}}T^{-3/2} \tag{6}$$

$$\frac{dT}{dt} = \frac{H_0'}{C_0}T^{-1/2}. \tag{7}$$

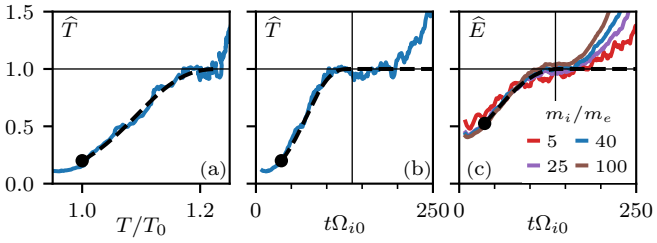

FIG. 4. Comparison with the resistive evolution model, $\widehat{T}$ as a function of (a) T and (b) time, and (c) $\widehat{E}$ as a function of time for several values of m_i/m_e. Solid lines are simulation data, dashed lines are the model predictions evaluated, and the model initial conditions are shown with a circle. For (a,b) the measured values $\gamma = 1/11$, $\bar{\alpha} = -3/5$ are used, with $C_0 = 5N_{SP,0}$ calculated from the simulation initial conditions and H_0' evaluated from Eq. (4). In (c), the model is developed based on the approximate power law quoted in the text. The vertical line in (b,c) shows the time estimated from Eq. (10).

The solution to these equations is

$$T = \left(\frac{3}{2}\frac{H_0'}{C_0}t + T_0^{3/2}\right)^{2/3} \tag{8}$$

$$\widehat{T} = F^{-1}\left(\frac{C_0}{\alpha_0}\ln\frac{T}{T_0}\right), \tag{9}$$

where $F(x) = \int_{\widehat{T}_0}^{x} t^{-1}(1-t)^{\bar{\alpha}}\,dt$. Collectively, these equations describe Ohmic heating and a collapse of the current sheet, but differ from previous results which assumed $T - T_0 \sim t$ and did not include a critical power law [24]. Setting $\widehat{T} = 1$ in Eq. (9) and using Eq. (8) and (4) leads to an estimate for the collapse timescale

$$\frac{\tau}{\tau_{A,0}} = \frac{5}{3}\left(e^{\gamma F(1)} - 1\right)\left(\frac{\delta_0}{\delta_{SP,0}}\right)^2 \tag{10}$$

where $\gamma \equiv 3\alpha_0/2C_0$. For initially thick current sheets, $\widehat{T}_0 \ll 1$ and $e^{\gamma F(1)} \approx (e^{1/\bar{\alpha}}\widehat{T}_0)^{-\gamma}$. In these simulations, $\gamma \approx 1/11$ and, assuming this is universal, $\tau \sim 10\tau_{A,0}$ for Sweet-Parker current sheets that are initially $10^4\rho_s$ thick, while for $\delta \lesssim 5\rho_s$, then $\tau \lesssim \tau_{A,0}$. This model is in good agreement with the simulation data, as shown in Fig. 4, however further study on the parameter and boundary condition dependence of γ is required before applying these predictions to other systems.

Although derived here in terms of $\widehat{T}$, an entirely equivalent analysis can be done in terms of $\widehat{E}$. For the simulations studied, an approximate power law, $\widehat{E}dH/d\widehat{E} \approx 0.13C_0(1-\widehat{E})^{-1/2}$ is found and the resulting model agrees well with all values of m_i/m_e tested, representative examples of which are shown in Fig. 4(c).

In the isothermal limit, $C \to \infty$, this model is identical to the slow-to-fast transition in the catastrophe model of Cassak *et al.* [14] where the Sweet-Parker current sheet is stable. This work extends the catastrophe

model by including thermodynamic feedback which results in an instability of the Sweet-Parker current sheet wherein Ohmic heating and thinning naturally drive the system towards collisionless regimes. This study does not address whether hysteresis is present in kinetic descriptions, and this remains an open question.

Here, a closed system with a single isolated current sheet was examined, however, in nature, current sheets do not occur in isolation. Additional thermodynamic effects such as thermal transport between the current sheet and the external environment or thermal coupling to neutrals [25] can modify these results. Furthermore, macroscopic physics can be more influential than local current sheet physics in determining current sheet stability and the long-term reconenction rate [40, 41], while microscopic kinetic physics can strongly influence stability in nearly collisionless systems.

Finally, in large collisional systems, fast reconnection is thought to be driven by the plasmoid instability [4, 6, 22], resulting in a fractal plasmoid chain that ends at either a Sweet-Parker or kinetic current sheet [7]. Previous estimates for the division between these two endpoints do not include the resistive evolution described here which will drive the terminating current sheet towards kinetic scales. Similarly, systems with initial Lundquist numbers below the critical value for plasmoid instability ($\sim 10^4$) can become plasmoid unstable due to self-consistent heating [5, 24]. Even without this modification, plasmoid instability itself is regarded as a separate reconnection phase, and future work will investigate whether it may be similarly understood as a phase transition and whether critical behavior is present.

The data that support the findings of this study are openly available in the Princeton University DataSpace [42].

The authors gratefully acknowledge funding from both the General Plasma Science Program from DOE Office of Fusion Energy Sciences and the Max Planck Princeton Center for Plasma Physics (MPPC) under DOE contract number DE-AC02-09CH11466.

The simulations presented in this article were performed on computational resources managed and supported by Princeton Research Computing, a consortium of groups including the Princeton Institute for Computational Science and Engineering (PICSciE) and the Office of Information Technology's High Performance Computing Center and Visualization Laboratory at Princeton University.

[1] J. Birn, J. Drake, M. Shay, B. Rogers, R. Denton, M. Hesse, M. Kuznetsova, Z. Ma, A. Bhattacharjee, A. Otto, *et al.*, Geospace environmental modeling (gem) magnetic reconnection challenge, Journal of Geophysical Research: Space Physics **106**, 3715 (2001).

[2] H. J. Cai, D. Q. Ding, and L. C. Lee, Momentum transport near a magnetic X line in collisionless reconnection, J. Geophys. Res. **99**, 35 (1994).

[3] W. Daughton, J. Scudder, and H. Karimabadi, Fully kinetic simulations of undriven magnetic reconnection with open boundary conditions, Phys. Plasmas **13**, 072101 (2006).

[4] N. Loureiro, A. Schekochihin, and S. Cowley, Instability of current sheets and formation of plasmoid chains, Physics of Plasmas **14**, 100703 (2007).

[5] W. Daughton, V. Roytershteyn, B. Albright, H. Karimabadi, L. Yin, and K. J. Bowers, Transition from collisional to kinetic regimes in large-scale reconnection layers, Physical review letters **103**, 065004 (2009).

[6] A. Bhattacharjee, Y.-M. Huang, H. Yang, and B. Rogers, Fast reconnection in high-lundquist-number plasmas due to the plasmoid instability, Physics of Plasmas **16**, 112102 (2009).

[7] H. Ji and W. Daughton, Phase diagram for magnetic reconnection in heliophysical, astrophysical, and laboratory plasmas, Physics of Plasmas **18**, 111207 (2011).

[8] P. Sweet, The neutral point theory of solar flares, in *Electromagnetic Phenomena in Cosmical Physics*, edited by B. Lehnert (Cambridge Univ. Press, New York, 1958) p. 123.

[9] E. N. Parker, Sweet's mechanism for merging magnetic fields in conducting fluids, J. Geophys. Res. **62**, 509 (1957).

[10] D. Biskamp, Magnetic reconnection via current sheets, Phys. Fluids **29**, 1520 (1986).

[11] H. Ji, M. Yamada, S. Hsu, and R. Kulsrud, Experimental test of the sweet-parker model of magnetic reconnection, Phys. Rev. Lett. **80**, 3256 (1998).

[12] F. S. Mozer, S. Bale, and T. D. Phan, Evidence of diffusion regions at a subsolar magnetopause crossing, Phys. Rev. Lett. **89**, 015002 (2002).

[13] Y. Ren, M. Yamada, S. Gerhardt, H. Ji, R. Kulsrud, and A. Kuritsyn, Experimental Verification of the Hall Effect during Magnetic Reconnection in a Laboratory Plasma, Phys. Rev. Lett. **95**, 055003 (2005).

[14] P. Cassak, M. Shay, and J. Drake, Catastrophe model for fast magnetic reconnection onset, Physical review letters **95**, 235002 (2005).

[15] M. Yamada, Y. Ren, H. Ji, J. Breslau, S. Gerhardt, R. Kulsrud, and A. Kuritsyn, Experimental study of two-fluid effects on magnetic reconnection in a laboratory plasma with variable collisionality, Phys. Plasmas **13**, 052119 (2006).

[16] B. Ö. Sonnerup, Magnetic field reconnection, Solar system plasma physics **3**, 45 (1979).

[17] B. Rogers, R. Denton, J. Drake, and M. Shay, Role of dispersive waves in collisionless magnetic reconnection, Physical Review Letters **87**, 195004 (2001).

[18] M. Yamada, R. Kulsrud, and H. Ji, Magnetic reconnection, Reviews of Modern Physics **82**, 603 (2010).

[19] P. Cassak, M. Shay, and J. Drake, A saddle-node bifurcation model of magnetic reconnection onset, Physics of Plasmas **17**, 062105 (2010).

[20] P. Cassak and J. Drake, On phase diagrams of magnetic reconnection, Physics of Plasmas **20**, 061207 (2013).

[21] Y.-M. Huang, A. Bhattacharjee, and B. P. Sullivan, Onset of fast reconnection in hall magnetohydrodynamics

mediated by the plasmoid instability, Physics of Plasmas **18**, 072109 (2011).
[22] W. Daughton, V. Roytershteyn, B. Albright, H. Karimabadi, L. Yin, and K. J. Bowers, Influence of coulomb collisions on the structure of reconnection layers, Physics of Plasmas **16**, 072117 (2009).
[23] W. Daughton, V. Roytershteyn, H. Karimabadi, L. Yin, B. Albright, S. Gary, and K. J. Bowers, Secondary island formation in collisional and collisionless kinetic simulations of magnetic reconnection, in *AIP Conference Proceedings*, Vol. 1320 (American Institute of Physics, 2011) pp. 144–159.
[24] A. Stanier, W. Daughton, A. Le, X. Li, and R. Bird, Influence of 3d plasmoid dynamics on the transition from collisional to kinetic reconnection, Physics of Plasmas **26**, 072121 (2019).
[25] J. Jara-Almonte, H. Ji, J. Yoo, M. Yamada, W. Fox, and W. Daughton, Kinetic simulations of magnetic reconnection in partially ionized plasmas, Physical review letters **122**, 015101 (2019).
[26] K. J. Bowers, B. Albright, L. Yin, B. Bergen, and T. Kwan, Ultrahigh performance three-dimensional electromagnetic relativistic kinetic plasma simulation, Physics of Plasmas **15**, 055703 (2008).
[27] K. J. Bowers, B. J. Albright, L. Yin, W. Daughton, V. Roytershteyn, B. Bergen, and T. Kwan, Advances in petascale kinetic plasma simulation with vpic and roadrunner, in *Journal of Physics: Conference Series*, Vol. 180 (IOP Publishing, 2009) p. 012055.
[28] T. Takizuka and H. Abe, A binary collision model for plasma simulation with a particle code, Journal of computational physics **25**, 205 (1977).
[29] J. Birn, M. Hesse, and K. Schindler, Entropy conservation in simulations of magnetic reconnection, Physics of plasmas **13**, 092117 (2006).
[30] H. Liang, P. A. Cassak, S. Servidio, M. A. Shay, J. F. Drake, M. Swisdak, M. R. Argall, J. C. Dorelli, E. E. Scime, W. H. Matthaeus, *et al.*, Decomposition of plasma kinetic entropy into position and velocity space and the use of kinetic entropy in particle-in-cell simulations, Physics of Plasmas **26**, 082903 (2019).
[31] S. Du, G. P. Zank, X. Li, and F. Guo, Energy dissipation and entropy in collisionless plasma, Physical Review E **101**, 033208 (2020).
[32] H. Liang, P. Cassak, M. Swisdak, and S. Servidio, Estimating effective collision frequency and kinetic entropy uncertainty in particle-in-cell simulations, in *Journal of Physics: Conference Series*, Vol. 1620 (IOP Publishing, 2020) p. 012009.
[33] P. Hall and S. C. Morton, On the estimation of entropy, Annals of the Institute of Statistical Mathematics **45**, 69 (1993).
[34] L. Kozachenko and N. N. Leonenko, Sample estimate of the entropy of a random vector, Problemy Peredachi Informatsii **23**, 9 (1987).
[35] T. B. Berrett, R. J. Samworth, M. Yuan, *et al.*, Efficient multivariate entropy estimation via k-nearest neighbour distances, The Annals of Statistics **47**, 288 (2019).
[36] See the Supplemental Material `SupplURL`, which includes Refs. [30, 32, 38, 39, 43–47].
[37] W. Daughton and V. Roytershteyn, Emerging parameter space map of magnetic reconnection in collisional and kinetic regimes, Space science reviews **172**, 271 (2012).
[38] M. M. Kuznetsova, M. Hesse, and D. Winske, Kinetic quasi-viscous and bulk flow inertia effects in collisionless magnetotail reconnection, Journal of Geophysical Research: Space Physics **103**, 199 (1998).
[39] M. Hesse, K. Schindler, J. Birn, and M. Kuznetsova, The diffusion region in collisionless magnetic reconnection, Physics of Plasmas **6**, 1781 (1999).
[40] A. Stanier, W. Daughton, L. Chacon, H. Karimabadi, J. Ng, Y.-M. Huang, A. Hakim, and A. Bhattacharjee, Role of ion kinetic physics in the interaction of magnetic flux ropes, Physical review letters **115**, 175004 (2015).
[41] J. Ng, Y.-M. Huang, A. Hakim, A. Bhattacharjee, A. Stanier, W. Daughton, L. Wang, and K. Germaschewski, The island coalescence problem: Scaling of reconnection in extended fluid models including higher-order moments, Physics of Plasmas **22**, 112104 (2015).
[42] J. Jara-Almonte and H. Ji, A thermodynamic phase transition in magnetic reconnection, `https://dataspace.princeton.edu/handle/88435/dsp01pz50gz45g` (2021).
[43] S. Braginskii and M. Leontovich, Reviews of plasma physics (1965).
[44] R. Schunk, Mathematical structure of transport equations for multispecies flows, Reviews of Geophysics **15**, 429 (1977).
[45] D. Biskamp, Instability of two-dimensional collisionless plasmas with neutral points, Plasma Physics **13**, 1013 (1971).
[46] J. Beirlant, E. J. Dudewicz, L. Györfi, and E. C. Van der Meulen, Nonparametric entropy estimation: An overview, International Journal of Mathematical and Statistical Sciences **6**, 17 (1997).
[47] J. Wygant, C. Cattell, R. Lysak, Y. Song, J. Dombeck, J. McFadden, F. Mozer, C. Carlson, G. Parks, E. Lucek, *et al.*, Cluster observations of an intense normal component of the electric field at a thin reconnecting current sheet in the tail and its role in the shock-like acceleration of the ion fluid into the separatrix region, Journal of Geophysical Research: Space Physics **110** (2005).